Characterising the stone artefact raw materials at Liang Bua, Indonesia

Sam C. Lin[1,2] [iD] **· Lloyd T. White[3] · Jatmiko[4] · I Made Agus Julianto[5] ·
Matthew W. Tocheri[2,5,6] · Thomas Sutikna[1,2]**

Abstract

At Liang Bua, the type site of *Homo floresiensis* on the Indonesian island of Flores, the stone artefact assemblages are dominated by two raw materials, qualitatively classified as chert and silicified tuff in previous studies. Field observations describe both stone types as locally abundant and of good flaking quality, but no systematic analysis has yet been carried out to characterise their nature. In this study, we conducted the first geological, mechanical, and quantitative assessment of these two raw materials using a suite of analytical approaches. Our results show that the two stone types are mineralogically alike in composition and derive from fossiliferous limestone that had undergone diagenetic silica replacement, but they clearly differ from one another geochemically. Therefore, the 'chert' and 'silicified tuff' categories used in previous studies are more aptly described as silica-dominated (i.e., SiO_2-dominated) nodular chert and iron-rich (i.e., Fe_2O_3-rich) nodular chert, respectively. We discuss the implications of our results on the shift in raw material utilisation patterns at Liang Bua that occurred after ~46 ka and coincided with the arrival of *Homo sapiens* at the site.

Keywords *Homo floresiensis* · *Homo sapiens* · Stone tools · Petrography · XRD · XRF · Hardness

Liang Bua is a large limestone cave on Flores, Indonesia (Fig. 1). The site, which has been excavated multiple times since 1965 (Morwood et al., [49], [50]), is well known as the type locality for *Homo floresiensis*, a hominin species with multiple primitive anatomical features, including small brain size and small body size (Brown & Maeda, [11]; Brown et al., [12]; Falk et al., [20]; Jungers et al., [27], [28]; Kaifu et al., [29], [30], [31]; Larson et al., [35]; Morwood et al., [49], [48]; Tocheri et al., [69], [70]). The skeletal remains of *H. floresiensis* recovered in this cave are dated

✉ Sam C. Lin
  samlin@uow.edu.au

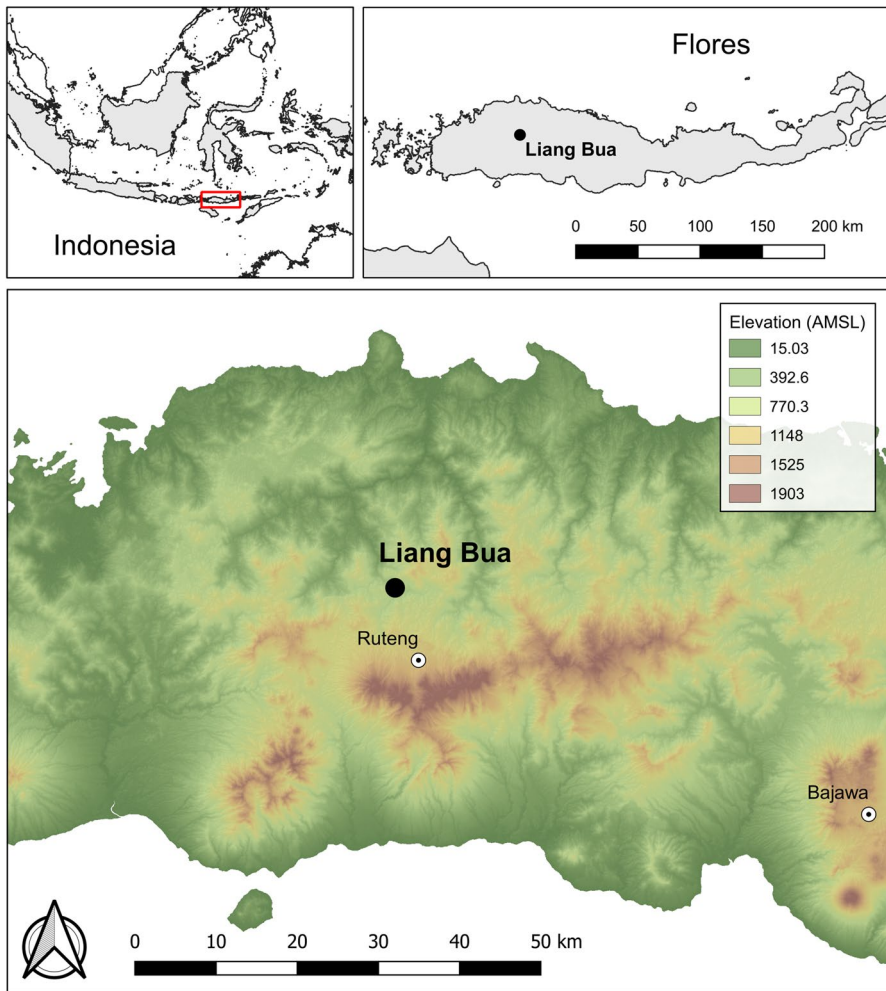Extended author information available on the last page of the article

Fig. 1 The geographic locations of Flores within Indonesia (top left) and Liang Bua on Flores (top right and bottom; AMSL, above mean sea level). Figure produced using QGIS (QGIS Development Team, [59])

to between ~ 100 and 60 thousand years ago (ka), and all cultural materials associated with this extinct hominin species span between ~ 190 and 50 ka (Sutikna et al., [68]). Subsequently, evidence of *Homo sapiens* (modern humans) first appears at the site ~ 46 ka and continues throughout the remainder of the stratigraphic sequence, which extends until the recent past with no major temporal gaps (Morley et al., [47]; Sutikna et al., [68], [67]). Both *H. floresiensis* and modern humans produced abundant archaeological assemblages that are the focus of the present study.

One of the intriguing features about the Liang Bua archaeological sequence is that, despite the apparent hominin turnover ~ 50–46 ka, the lithic assemblages exhibit minimal change in terms of the stone reduction pattern over time (Moore

et al., [46]). Instead, stone artefacts at the site are characterised by a flaking process in which larger flakes and cores were transported to the cave and reduced centripetally and bifacially to produce smaller flakes (Moore, [43]; Moore & Brumm, [44], [45]; Moore et al., [46]). Similar flaking patterns have also been documented elsewhere in eastern Indonesia (Marwick et al., [41]; Shipton et al., [66]), including at the So'a Basin in central Flores between at least 1.02 million years ago and ~700 ka (Brumm et al., [13], [14], [15]), suggesting long-term technological continuity in the greater region, at least in terms of flake production strategies (Moore, [43]; Moore & Brumm, [44], [45]; Moore et al., [46]; Shipton et al., [66]). However, other aspects of the archaeological sequence at Liang Bua indicate that some behavioural changes occurred following the initial appearance of modern humans on the island. For instance, clear microstratigraphic signs of anthropogenic combustion are present ~41–24 ka, suggesting controlled fire use among Late Pleistocene modern humans utilising the cave, behaviours not yet documented for *H. floresiensis* (Morley et al., [47]) despite initial claims otherwise (Morwood et al., [49], [48]). In addition to controlled fire use, an increase in edge-polished flakes also occurs at the site during the terminal Pleistocene and Holocene (Moore et al., [46]). Recent experiments have suggested the possibility that these edge-polish flakes were used for processing siliceous plant materials, such as palm and bamboo, in the upper part of the stratigraphic sequence (Hayes et al., [25]).

Lithic raw material usage is another aspect of the Liang Bua archaeological sequence that exhibits remarkable change. The stone artefacts at Liang Bua are primarily made from two raw materials, silicified tuff and chert (Moore et al., [46]; Sutikna et al., [67]); other stone types, including silicified limestone, chalcedony, jasper, andesite, and quartz, are represented in considerably lower frequencies (Sutikna et al., [67]). The silicified tuff and chert are both noted to be available as cobbles (albeit in unknown quantities) in the Wae Racang, a river that flows ~200 m north of the cave today (Moore et al., [46]). Moore et al. ([46]) reported that within the Pleistocene stone artefact assemblage at Liang Bua, which was thought at that time to be exclusively associated with *H. floresiensis*, 83.4% of the 8388 artefacts studied were made of silicified tuff, whereas the remaining 16.6% was made of chert. In comparison, the proportion of chert artefacts in the Holocene assemblage, which is exclusively associated with modern humans, surged to 61.6% of the 2861 artefacts studied, while the silicified tuff proportion fell to 38.4% (Moore et al., [46]). Moore et al. ([46]) noted that many of the chert artefacts from the Holocene assemblage contain patches of soft, chalky cortex, suggesting that these chert materials were obtained from bedrock or colluvial sources rather than the Wae Racang gravel bed. They further argued that the observed shift in raw material selection at Liang Bua was part of a suite of adaptive behavioural changes associated with the arrival of modern humans to Flores (Moore et al., [46]).

In a more recent study, based on the revised site stratigraphy (Sutikna et al., [68]) and a study sample that was different from that used by Moore et al. ([46]), a similar raw material pattern was observed (Sutikna et al., [67]). Specifically, the *H. floresiensis* lithic assemblage (from stratigraphic units 1A, 1B, and 2 combined) was dominated by artefacts made from silicified tuff (69.9% of the 4419 artefacts studied), whereas the use of chert remained relatively low (17.2%). In comparison, among the lithic assemblages

dated to after~46 ka (from stratigraphic units 4, 5, 6, 8A, 8B, 8C combined), the proportion of silicified tuff artefacts decreased notably (34.4% of the 6015 artefacts studied) while that of chert artefacts increased (45.3%). Sutikna et al. ([67]) suggested that this shift in raw material usage reflects that the modern humans using Liang Bua after~46 ka may have selectively acquired and transported chert materials from more distant sources, leading to a larger amount of chert artefacts being produced and discarded in the cave. In contrast, because silicified tuff occurs in abundance in the nearby Wae Racang, the high proportion of silicified tuff artefacts prior to 50 ka may indicate a greater reliance by *H. floresiensis* on stone raw materials that were more readily available around the site (Sutikna et al., [67]).

If the increased prevalence of chert at Liang Bua after~46 ka was related to modern human raw material preference, the reason for why this was the case is not immediately obvious. Discussions of lithic raw material selection often highlight the trade-offs between procurement cost and raw material properties associated with fracture predictability and flake production (Andrefsky, [3]; Brantingham et al., [9]). Put simply, stones with more predictive fracture patterns can afford toolmakers greater control over the knapping process. As such, it is commonly assumed that fine-grained stone types, such as chert, would have been preferred over coarser-grained materials by past toolmakers. However, at Liang Bua, researchers have observed no obvious difference in the flaking quality of the locally available chert and silicified tuff, both of which have been described as relatively fine-grained and of high flaking quality (Moore et al., [46]). Such similarities in flaking quality between these two raw materials may help explain the overall lack of difference in the way these were both knapped by hominins (Moore et al., [46]). Taking these observations together, the systematic increase in chert artefacts discarded by modern humans at Liang Bua may involve factors beyond fracture predictability. One possibility is that chert was selectively exploited for functional considerations. Recent studies have demonstrated that functional attributes, such as edge sharpness and durability, may be as important, if not more so, as fracture predictability for past raw material selection and transport (Abrunhosa et al., [1]; Braun et al., [10]; Key, [32]; Key et al., [33]; Lemorini et al., [36]; Seong, [62]). As noted earlier, the arrival of modern humans at Liang Bua resulted in some changes in the hominin activities represented at the site, including the possible increased occurrence of plant processing based on the edge-polished flakes (Hayes et al., [25]; Moore et al., [46]). It may thus be that flakes made from chert outperform those made from silicified tuff in carrying out these tasks.

To begin evaluating these hypotheses of raw material selection and hominin behaviour at Liang Bua, it is first necessary to develop a better understanding of the geological and mechanical properties of the chert and silicified tuff represented in the stone artefact assemblage (Moore et al., [46]; Sutikna et al., [67]). Specifically, if the variation in raw material usage at the site was related to the production and/or function of stone tools, then we would expect the chert and the silicified tuff to exhibit differences in their mineralogy and mechanical characteristics that can impact their flakability and functional performance. Beyond categorical classifications, no analysis has yet been carried out to quantitatively characterise these two stone types. In this study, we conduct a suite of petrographic, crystallographic,

geochemical, and mechanical analyses on samples of chert and silicified tuff collected in the Liang Bua vicinity to investigate the nature and physical characteristics of these two lithic raw materials.

Material and Methods

Liang Bua is located in the Waihekang Formation, an area marked by a Pliocene-Miocene tuffaceous clastic limestone that is minimally compact and porous, making it susceptible to rapid karstification (Koesoemadinata et al., [34]; Nanlohy et al., [53]; Westaway et al., [73]). Moore et al. ([46]) suggested that the silicified tuff represented at Liang Bua was formed through submarine volcanic eruptions that deposited the local tuff-bearing clastic limestone. This stone type is said to exist in great abundance in the Wae Racang near Liang Bua today (Moore et al., [46]). Similar green-coloured silicified tuff is apparently widespread elsewhere on Flores (Harahap et al., [24]), and artefacts made from the stone type have also been reported from the Middle Pleistocene site of Mata Menge in the So'a Basin (Brumm et al., [15]). As for chert, while previous studies have noted its occurrence in river gravels and bedrock exposures around Liang Bua (Moore et al., [46]; Westaway et al., [73]), there is limited information concerning the material's nature and occurrence.

To obtain samples of the two stone types for analysis, we conducted pedestrian surveys along a section of the Wae Racang ~ 200 m north of Liang Bua, as well as in the inland area surrounding the site (Fig. 2). Note that our goal here was to obtain samples to carry out detailed geological and mechanical analysis, rather than to summarise systematically the distribution of the two raw materials on the landscape. As such, we opted for an opportunistic survey approach guided by local community members. We recognise that, unlike probabilistic or systematic sampling (Banning, [4]), this survey approach carries inherent bias, such that the survey outcome is in no way representative of the overall raw material distribution. However, given the limited prior information regarding the raw materials, especially for chert, as well as other logistical constraints, including very poor surface visibility due to dense vegetation cover, relying on local community knowledge was the best solution to obtain the samples for our study purposes.

In the sections of the Wae Racang gravel bed that were surveyed, the size of the silicified tuff encountered ranged widely from large boulders to small pebbles. We collected several samples that exhibited a range of colour variation in the alluvial cortex (pale/greyish green to brown; Fig. 3a b). Some of the variations observed for this stone type may reflect differences in weathering, as there were examples of in situ weathering of silicified tuff cobbles on the riverbed (Fig. 3c). Importantly, test flaking of the collected samples showed an internal colour of varying shades of blue-green (Fig. 3d) or dark brown that was consistent with the silicified tuff artefacts identified in the Liang Bua assemblage (Fig. 4a-d).

As mentioned above, Moore et al. ([46]) suggested that the chert represented in the Liang Bua assemblage was acquired mainly as cobbles from the Wae Racang gravel beds. However, we encountered very few chert stones along the river, all of which were small pebbles. On the other hand, we identified small to medium
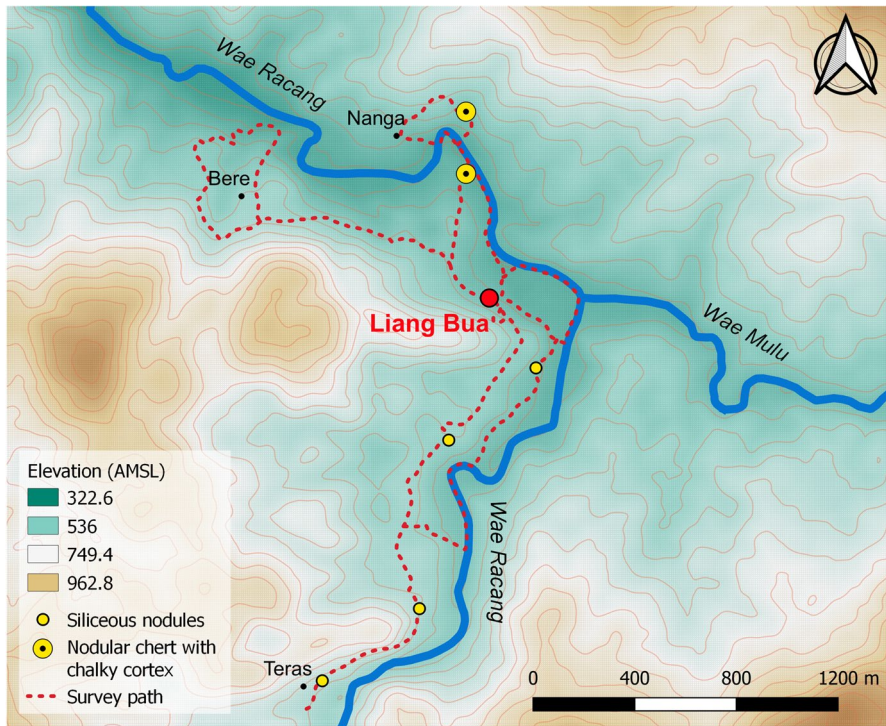
Fig. 2 The pedestrian survey paths with respect to the geographic location of Liang Bua and its surrounding rivers. The contour lines are drawn with a 20 m interval (AMSL, above mean sea level). Figure produced using QGIS (QGIS Development Team, [59])

cobbles of wine-red jasper and chalcedony among the gravel beds, with a cortex and internal colour that were similar to those observed on the same material types in the Liang Bua assemblage. However, these jasper and chalcedony cobbles are not part of the present study as they are relatively rare at Liang Bua (< 10% among the stratigraphic units) in comparison to the two dominant raw materials, silicified tuff and chert. Instead, the qualitative lack of chert from the riverbed observed from our survey suggests the possibility that past hominins in the region obtained this raw material elsewhere among the surrounding limestone landscape. This scenario is supported by the presence of chalky cortex on some of the chert artefacts at Liang Bua (Fig. 4f g), suggesting that the material may have been acquired from exposed bedrock or colluvial sources (Moore et al., [46]). Based on information from local residents that chert nodules are occasionally encountered in local gardens during soil tilling, we surveyed the paths between Liang Bua and two nearby villages, Teras to the south and Bere to the west (Fig. 2). The survey examined a series of limestone sections and soil profiles exposed by road cut, mostly to the south toward Teras. Although a limited number of isolated siliceous nodules were identified in these exposed sections, no chert was recovered along these survey paths. Note that we also did not observe any silicified tuff during the survey away from the river
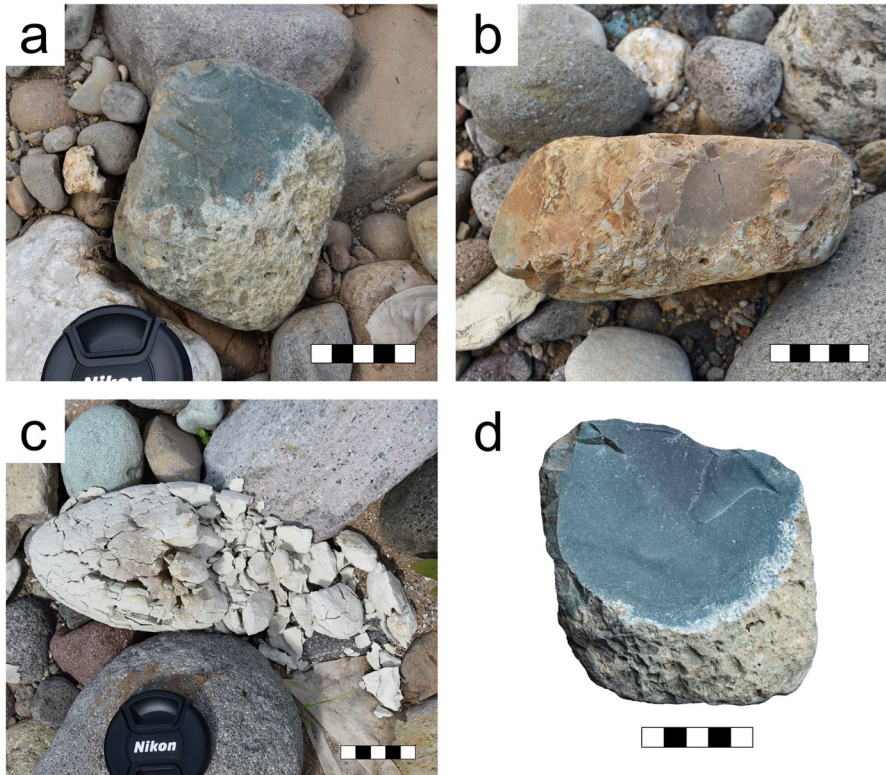
Fig. 3 Silicified tuff samples recovered during the survey: **a**, **b** silicified tuff nodules observed in the Wae Racang cobble bed; **c** in situ weathered silicified tuff nodule; **d** test flaking of a silicified tuff sample exposes a blueish green interior colour. Figure produced using Inkscape (Inkscape Project, [26])

gravel bed, suggesting that the material may only occur as alluvial material in the river and not in the surrounding limestone hills.

In their study, Moore et al. ([46]) mentioned the presence of a Neolithic site, Golo Roang, located about 500 m northeast of Liang Bua across the Wae Racang. The site contains Neolithic adze blanks and adze manufacturing debitage made from a beige chert with a dull to matted lustre (see Fig. 32 in Moore et al. ([46])), which is similar to the chert represented at Liang Bua (Fig. 4e-g). It thus stands to reason that there may be a source of chert located north of Liang Bua. To evaluate this possibility, we surveyed north of Liang Bua and identified two locations with a greater occurrence of chert. At ~ 500 m northwest of Liang Bua, along the south bank of the Wae Racang, multiple medium to large chert nodules with chalky cortex were identified on the ground and within garden retaining walls (Fig. 5a). Farther to the north across the river, large quantities of nodular chert were found littered on the lower river terrace east of Nanga village (Fig. 5b). At both locations, the chert nodules had irregular forms with 'knobby' surfaces, chalky white weathering rind, and fossil burrow features (Fig. 5d) that are typical of nodular
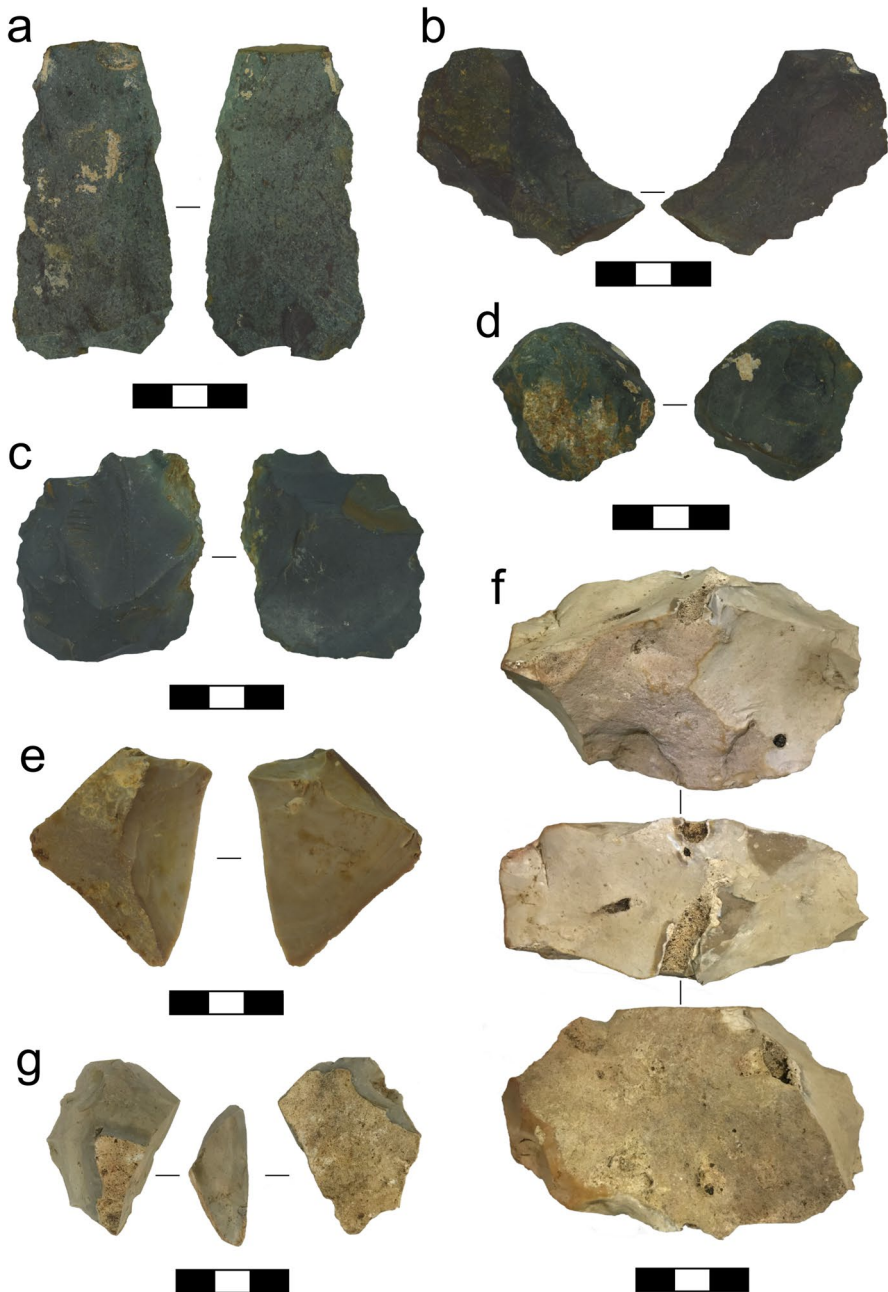
Fig. 4 Examples of silicified tuff (**a–d**) and chert (**e–g**) artefacts from Liang Bua: **a**, **e** complete flakes; **b** complete flake with denticulate retouch; **c**, **d** flake blank cores (or core-on-flakes); **f** orthogonal core; **g** truncated flake. Figure produced using Inkscape (Inkscape Project, [26])
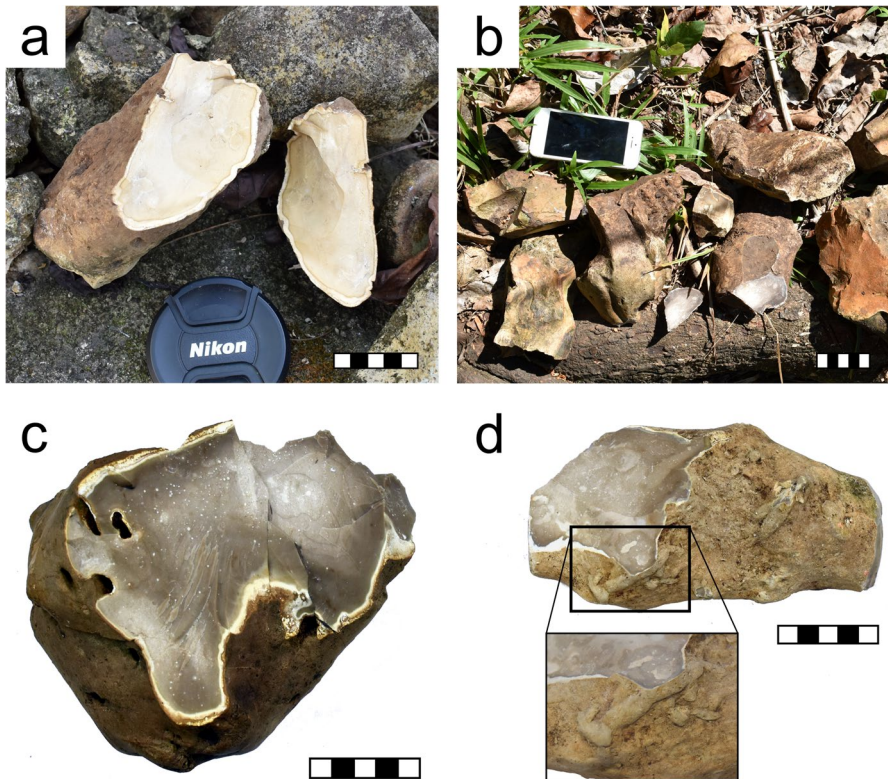
Fig. 5 Chert samples recovered during the survey: **a**, **b** chert nodules with chalky cortex identified north of Liang Bua; **c** test flaking of a chert sample exposes a greyish-brown interior colour; **d** a chert sample exhibiting fossil burrow features on the exterior. Figure produced using Inkscape (Inkscape Project, [26])

chert originating from diagenetic silica replacement in carbonate rocks (Boggs, [7]; Maliva & Siever, [39]). Visual inspections of test flaking results suggest that the chert nodules share similar physical characteristics (e.g. beige colour with dull lustre and opaque translucency, or greyish-brown colour with shiny lustre) to those represented in the Liang Bua lithic assemblage (Fig. 4e-g). The chert samples analysed in this study are materials collected from these two locations.

Among the raw materials sampled, we selected eight chert (C1–C8) and three silicified tuff (ST1–ST3) nodules for detailed geological and mechanical analyses (Table S1). While the sample size is limited, our analyses provide a suite of comprehensive information that are useful as a first step toward quantitatively characterising the nature of the two dominant lithic raw materials recovered at Liang Bua.

Comparison with Archaeological Specimens

As mentioned above, the raw material samples collected in our survey share similar visual characteristics to the stone artefacts at Liang Bua that have been

identified as the same stone types. To further verify that our geological samples correspond to the archaeological raw materials, we conducted portable X-ray fluorescence (pXRF) analysis to compare the geochemistry of the raw material samples analysed in this study to those of Liang Bua stone artefacts identified in previous studies as chert and silicified tuff. Although comparisons of the accuracy and precision of pXRF units with other lab-based geochemical methods have produced variable results (e.g., Grave et al., [22]; Sheppard et al., [63]), the non-destructive nature of pXRF is useful for making direct geochemical comparisons between raw material samples and archaeological artefacts. However, given the uncertainties surrounding the accuracy of pXRF, the comparisons here were carried out in relative terms. In other words, we focused on examining the relative differences/similarities rather than the absolute values of the elemental concentrations between the geological and archaeological samples.

To carry out the analysis, we used a Thermo Scientific Niton XL3t GOLDD + pXRF unit fixed in a mobile testing stand. The pXRF device is equipped with a silver (Ag) anode X-ray tube (6–50 kV, 0–200 µA max.), with the X-rays calibrated using the 'TestAll Geo' setting that automatically determines between the Compton normalization calibration and the fundamental parameters calibration, depending on the total metal content of the samples analysed. Elemental composition is output by default in terms of both parts per million (mg/kg), or ppm, and percent of composition by weight, with 0.10% being the cut-off point. Here we report the pXRF measurements for several major elemental oxides and trace elements (K_2O, CaO, TiO_2, MnO, Fe_2O_3, Cu, Zn, Rb, Sr, Zr, and Pb) that have been shown to yield reliable values by pXRF (Hall et al., [23]) and also consistently produced readings during our analyses.

For the raw material samples, the standard analysis protocol used here involved testing a clean flat surface cut by a diamond saw for 180 s (Newlander et al., [54]). A similar analytical protocol was applied to a collection of archaeological stone artefacts from Liang Bua using the flattest surface on each artefact. This artefact collection, which is temporarily on loan to the University of Wollongong by the Archeometry Research Center of the Indonesian Archaeological, Language, and Literary Research Organization, contains 27 chert and 28 silicified tuff artefacts that each weighs more than 1 g and has a relatively flat surface that covers the entirety of the instrument test window. A certified powder standard, CCRMP TILL-4PP (180–646), was routinely analysed between measurements of the artefact samples to monitor the pXRF performance. A summary of the results obtained from measurements of the standard are provided in Table S2, together with the certified values for comparison.

Geological Analysis

To further characterise the nature of the raw material samples in detail, the samples were thin-sectioned and examined using a Leica DM2500 P petrographic microscope at the University of Wollongong to characterise their mineralogy, grain size,

and other distinguishing features. In addition, approximately 50 g of a representative component of each raw material sample was pulverised using a tungsten-carbide ring mill for 60 s. A 20 g aliquot of each pulverised sample was set aside for X-ray fluorescence (XRF), and < 1 g of this material was used for X-ray diffraction (XRD) after it was ground further by hand using an agate mortar and pestle for ~ 60 s. Dilute hydrochloric acid (HCL) was applied to the raw material hand samples as well as the pulverised samples to determine their reaction to acid.

X-Ray Diffraction The diffraction patterns were obtained using a Thermo Fisher Equinox 1000 asymmetric/curved X-ray diffractometer at the University of Wollongong. The diffractometer is equipped with a copper long-fine-focus X-ray source. Samples were measured on a rotating stage (nine revolutions per minute) over 120 min, using a 2 mm × 0.1 mm aperture and 4° incidence angle. Spectra were obtained between 4 and 110° 2-theta. Phase identification was completed using the International Centre for Diffraction Data (ICDD) PDF-2-Minerals database and the software 'Match!' (version 3.10.2.173). Where more than one mineral phase was detected, estimates of the modal percentages of each phase were determined using the direct derivation method (Toraya, [71]).

X-Ray Fluorescence The whole-rock major and trace element composition of each sample was determined using a Spectro Ametek XEPOS III energy dispersive XRF spectrometer at the University of Wollongong. Trace element data were measured using pressed powder pellets (each pellet using ~ 5 g of pulverised sample combined with ~ 10 drops of PVA solution and pressed into an Al cup at 2500 psi). The pressed pellet was dried at 70 °C for > 2 h and then weighed to two decimal places. Major element data were obtained from the analysis of glass-fusion beads using one of two fluxes (pure Lithium Metaborate or a 57:43 mixture of lithium metaborate and lithium tetraborate) which were selected according to an assessment of the concentration of Si, Ca, and Fe in each sample estimated from an analysis of the pressed pellet. The glass beads were made using ~ 0.4 g of powdered sample material and ~ 4 g of flux. Samples with > 1000 ppm S or > 300 Cu were oxidised using 5 ml of lithium nitrate prior to preparation of the glass fusion bead to prevent damage to platinum crucibles used to prepare the glass beads. Two geological reference materials were run as unknowns alongside the raw material samples to ensure the accuracy of results. The iron concentration for each sample is reported as total Fe_2O_3. The major element data were reduced using a loss-on-ignition (LOI) measurement, where each sample was weighed before and after heating to 1100 °C for > 2 h. The results are reported on a volatile-free basis.

We focused our analysis on two groups of elements. The first group includes Ti, Zr, and Th, which are relatively immobile during post-depositional alterations and are indicators of the depositional environment in which the stones originally formed (Murray, [51]). Although Fe and Al in chert have also been previously suggested to be minimally affected by diagenesis (Murray, [51]), studies have shown that both elements can be affected by secondary alterations (Gauthier et al., [21]; Sheppard & Pavlish, [64]). The second group includes Sr, Mn, Cl, Ca, Mg, Ba, Na, K, P, and Rb,

which tend to be mobile and are hence useful for gauging the variation in the degree of secondary alteration among the raw material samples (Malyk-Selivanova et al., [40]; Murray, [51]; Sheppard & Pavlish, [64]).

Mechanical Analysis

Density The density of each raw material sample was calculated by first determining their volume from a 3D model obtained using a structured light scanner (Polyga Compact C210 and the FlexScan3D software), then dividing the volume by the weight of the scanned sample, measured to the nearest 0.1 g. Before scanning and weighing, the cortex was cut from the raw material samples using a diamond saw. This is because the density of the outer weathering rind of the stones would be differentially affected by the degree of weathering. Here we focus on comparing the density measure of the inner non-cortical part of the samples. The extent of the cortex layer and its interface with the non-cortical stone was determined by changes in colouration, which is generally abrupt among the samples (e.g. Figure 5c, d).

Rebound Hardness Analysis Rebound hardness measures the hardness of the raw material in relation to elasticity, that is, the ability to change shape temporarily and return to the original shape when the pressure is removed. A rebound hardness test drops a diamond-tipped hammer from a fixed height onto the test material and measures the elevation/velocity of the rebound. Rebound hardness has been shown to correlate with elastic parameters like Young's modulus among some stone types (Aldeeky et al., [2]; Wang et al., [72]), with higher values of rebound hardness indicating greater material stiffness. Moreover, rebound hardness correlates with the homogeneity of rocks (measured by the frequency of impurities and microscopic cracks) as well as their ability to withstand strain (Braun et al., [10]; Yaşar & Erdoğan, [75]). As such, studies have employed rebound hardness as a proxy for flakability and fracture predictability of lithic raw materials (Egeland et al., [18]; Noll, [55]).

We tested the rebound hardness of the chert and silicified tuff samples using a pen type Leeb hardness tester (TIME 5100) with a 'D' impact device and a tungsten carbide tip. The impact body (i.e. the hammer) within the tester was loaded by a spring mechanism and then released to hit the material surface. The impact and rebound velocity of the impact body was determined at a distance of 1 mm from the material surface based on the voltage generated by the coil inside the device. The rebound hardness of the material, expressed in the scale of HLD, was calculated by the ratio of the rebound velocity and the impact velocity multiplied by a factor of 1000. Prior to testing, the raw material samples were cut by a diamond saw to have two parallel flat surfaces. Because all of the cut samples were relatively small (<2 kg), the samples were coupled on a 10 kg cast-iron anvil by first filling the contacts between the samples and the anvil with industrial grease and firmly pressing the samples down

onto the anvil. The Leeb test was then carried out by holding the hardness tester downwards perpendicularly to the flat sample test surface. For each sample, a total of 10 measurements were taken at different points of the test surface to determine the average rebound hardness value.

Indentation Hardness Analysis Indentation hardness quantifies the hardness of the raw material related to plastic deformation. The test is done by indenting a standardised sharp tip into the surface of the test material under a known load, then measuring the resulting indented impression. Studies have shown that stone raw materials with higher indentation hardness tend to be constituted of smaller grains with less porosities and lower surface roughness, potentially allowing flakes to be detached with sharper edges and hence greater cutting abilities (Yonekura, [76]; Yonekura & Suzuki, [78]). Researchers have also used indentation hardness as a proxy for tool edge durability (Sherwood, [65]; Yonekura, [76]; Yonekura et al., [77]), although it should be noted that edge toughness is proportional to not only indentation hardness but also stiffness, such that hard yet stiff (i.e. highly brittle) stones can in fact have low edge toughness (McPherron et al., [42]).

We tested the indentation hardness of the raw material samples using the Koop hardness test. The Knoop test uses an elongated pyramid indenter that allows only a small indentation to be made during testing, making the test particularly suited for very hard and brittle materials, such as glass and ceramic. The indentation hardness of the material, expressed in the scale of HK, was calculated as the ratio of the input load and the area of the indented impression. To conduct the test, small parallel-plane slices of each raw material were cut using a precision saw. Each sample was indented nine times (following a 3×3-mm grid) on the test surface using the Matsuzawa Via-F hardness tester at the University of Wollongong. Following Namen et al. ([52]), the indentations were made using a load of 10 kgf (or 98.07 N), a speed of 1 mm per s, and a hold time of 20 s. The length of the indentations along the long axis was measured using the ImageJ software (Schneider et al., [61]) on images of the tested samples captured by the Phenom XL scanning electron microscope. The Knoop hardness value (GPa) was calculated with the following:

$$HK = 0.0142F/L^2$$

where F is the applied load in Newtons, and L is the length of the long diagonal of the indent in millimeters.

The data were analysed using the R statistical software (R Core Team, [60]). We employed the Kendall rank correlation coefficient to examine correlations among the variables. Because of the small sample size evaluated here, we use the Mann–Whitney U test (bootstrapped over 1000 iterations) and the resulting 95% confidence interval of the p-value to assess two-sample differences. An alpha value of 0.05 was used to assign test significance. The data and R code for reproducing the figures and statistical findings are archived on the open online repository Zenodo (10.5281/zenodo.7145681).

Results

Portable X-Ray Fluorescence

The pXRF measurements are summarised in Table S3 for the raw material samples and in Tables S4 and S5 for the archaeological samples. Overall, the relative geochemical pattern of the raw material samples analysed here matches well to that of the archaeological stone artefacts. The geological samples ST1–ST3 and archaeological samples attributed to silicified tuff consistently show more elevated concentrations of K_2O, TiO_2, MnO, Fe_2O_3, Zn, Rb, Sr, Zr, and Pb than those attributed to chert. In comparison, for the geological samples C1–C8 and archaeological specimens classified as chert, the amount of Zn, Rb, Zr, and Pb is generally under the limits of detection and cannot be reliably measured. Some of these geochemical variations can consistently discriminate between the two raw material groups among the geological and archaeological samples. For example, Fig. 6 compares the concentration of Fe_2O_3, K_2O, and TiO_2 (in natural logarithmic scale) between the raw material samples and the analysed stone artefacts. The artefacts identified qualitatively as silicified tuff produced values that overlap with the range observed on ST1–ST3, while values from artefacts identified qualitatively as chert overlap with the range observed on C1–C8. The close agreement between the two sets of data suggests that the raw material samples examined here reasonably correspond to the two dominant lithic raw materials identified in the archaeological assemblage at Liang Bua.

Petrographic Analysis

The chert samples examined (C1 and C4) contain numerous foraminifera (50–1500 μm) and algal materials (up to 1.5 mm) that have been replaced with very
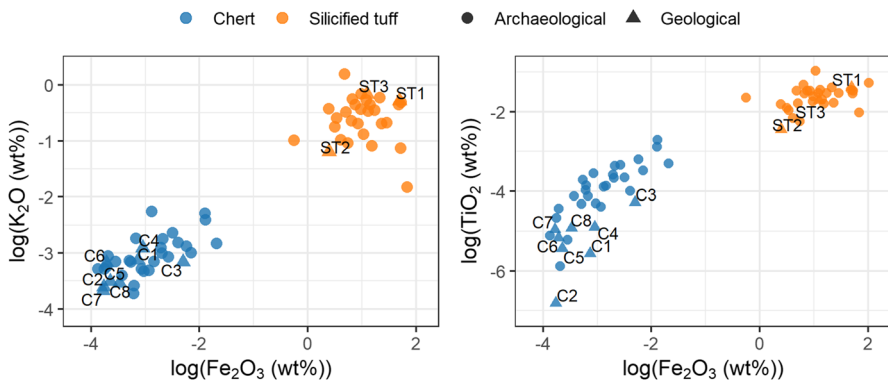

Fig. 6 Comparison of Fe_2O_3, K_2O, and TiO_2 (transformed by natural logarithm) measured by pXRF on the raw material samples and a collection of archaeological stone artefacts from Liang Bua. The labels denote the position of the geological samples on the plots. Figure produced using the R statistical software (R Core Team, [60])

fine SiO_2 and opaque minerals (Fig. 7a-c). These replaced foraminifera and algal materials represent from ~ 1–2 to 10% of the examined samples. C1 further contains secondary SiO_2 mineralisation that filled existing pore space and/or replaced primary minerals, resulting in features that resemble angular quartz grains and quartz veinlets (Fig. 7b). The matrix of the chert samples is generally very fine-grained (< 50 μm) and difficult to determine optically, but is most likely very fine-grained quartz and opaque minerals (potentially iron minerals) (Fig. 7b). The finer-grained,
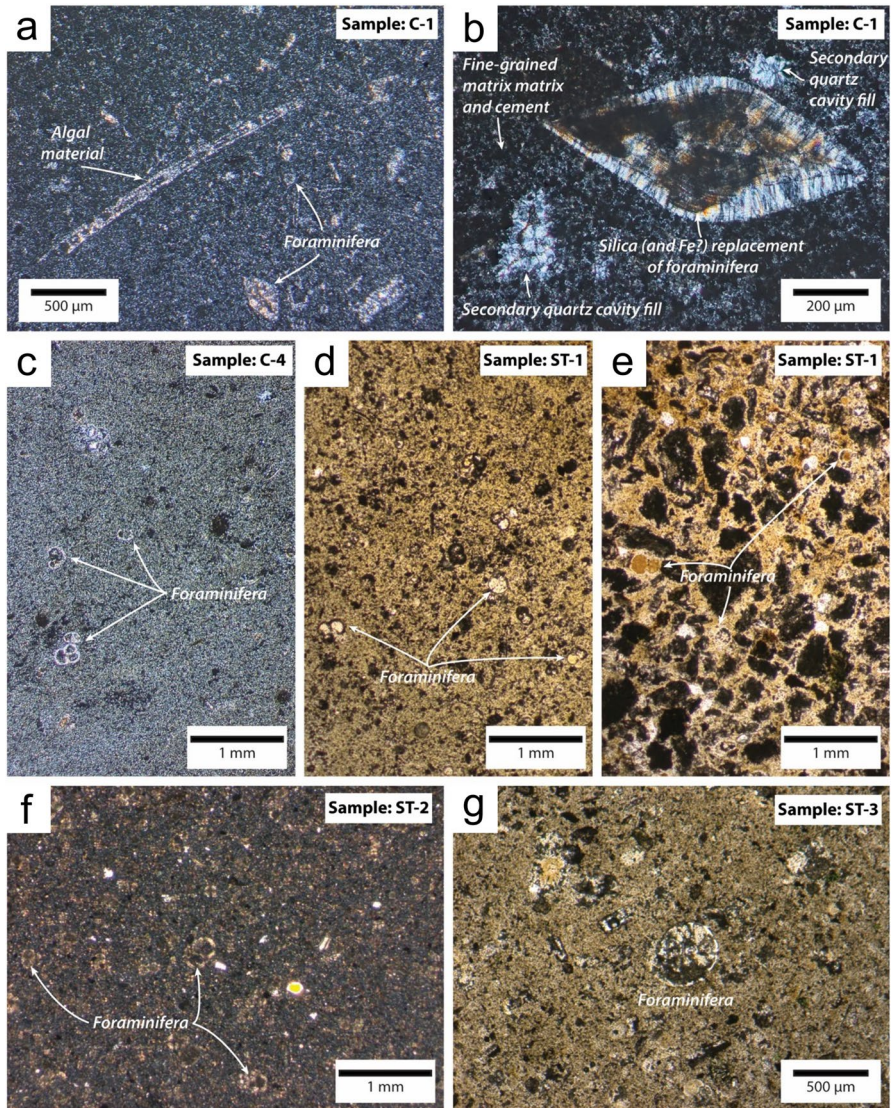

Fig. 7 Petrographic thin sections showing microstructures of the chert (**a–c**) and the silicified tuff (**d–g**) samples examined here. Figure produced using Inkscape (Inkscape Project, [26])

matrix-supported sections of the samples were originally a sparse biomicrite (Folk limestone classification) that has since been diagenetically altered/replaced by silica or carbonate cement.

Samples ST1–ST3 also include numerous SiO_2 replaced foraminifera (50 to 600 μm) and algal material, which represents 5 to 10% of these samples (Fig. 7d-g). These samples contain occasional angular quartz (< 1–5%) grains with sizes ranging between ~ 20 and 250 μm. The matrix of the samples ST1–ST3 is most likely composed of quartz, but since the matrix is very fine-grained (< 50 μm), it is difficult to determine optically. In contrast to the silicified tuff classification based on field observations, the finer-grained, matrix-supported sections of the samples suggest these stones were originally a sparse biomicrite (folk limestone classification) that has since been diagenetically altered/replaced by silica or carbonate cement. Some samples also include compositional bands that contain a higher proportion of clasts and are clast supported (Fig. 7e). Remnants of clasts that have been totally replaced by very fine-grained quartz with sizes ranging between 50 and 500 μm are also visible. These coarser, clast-supported sections, which also contain (1) angular quartz fragments (~ 5% of the samples); (2) 100–500 μm foraminifera (~ 5% of the samples), and (3) show clear signs of silica replacement, were likely an unsorted biosparite (folk limestone classification) or a volcaniclastic unit that were deposited in a shallow marine environment. However, regardless of the depositional environment of these clast-supported sections, the original minerals have since been diagenetically altered/replaced by silica.

X-Ray Diffraction

The XRD results, which are summarised in Table 1, indicate that all of the examined samples were dominated by quartz (SiO_2). Some of the samples contained minor amounts of siderite ($FeCO_3$) and/or calcite ($CaCO_3$) and potentially other clay mineral phases such as chloritoid or perhaps illite, and one sample (ST-3) potentially contained trace amounts of copper sulphide ($CoSO_4$).

Hydrochloric Acid Test

The reactions of the raw material samples to hydrochloric acid correlate with the presence of calcite as identified by the XRD results. Most of the chert samples had either a delayed reaction, or no reaction at all (Table S6). This reflects the fact that these samples are almost entirely composed of quartz, with minimal, if any, calcite present (which may be below the XRD detection level). The exception is C7, where the higher calcite percentage (1.8%; Table 3) explains its immediate response to HCL as a powdered sample. Similarly, ST1–ST3 also had faster reactions to HCL, corresponding to their higher amounts of calcite ($CaCO_3$) according to the XRD results (Table 1).

Table 1 Summary of the results from the XRD analyses

Sample ID	Mineral 1 (estimated %)	Mineral 2 (estimated %)	Mineral 3 (estimated %)
C1	Quartz (100%)	-	-
C2	Quartz (100%)	-	-
C3	Quartz (100%)	-	-
C4	Quartz (100%)	-	-
C5	Quartz (100%)	-	-
C6	Quartz (100%)	-	-
C7	Quartz (98.2%)	Calcite (1.8%)	-
C8	Quartz (100%)	-	-
ST1	Quartz (94.5%)	Siderite (4.4%)	Calcite (1.1%)
ST2	Quartz (96.2%)	Calcite (3.8%)	-
ST3	Quartz (99.8%)	Copper sulphide (0.2%)	-

X-Ray Fluorescence

Tables 2 and 3 summarise the XRF results. In line with the findings earlier, all of the samples are composed primarily of SiO_2 (>79%) with limited CaO. This result again suggests that, despite their different field classifications, both raw material types were originally fossiliferous limestone that was later diagenetically altered by silica replacement of existing carbonate. Nonetheless, echoing the differences outlined earlier with the pXRF results, there are notable variations in the geochemistry between these two raw material groups. Namely, the amount of SiO_2 (79–86%) in ST1–ST3 is lower than those among C1–C8 (89–98%), while ST1–ST3 have relatively higher concentrations of Fe_2O_3 (1.6–5.2%) than C1–C8 (<0.06%) (Fig. 8). Overall, there is a negative correlation between SiO_2 and Fe_2O_3 (Kendall's tau = −0.66, $p = 0.005$). The concentrations of the other major elements are all very low (generally <1%) across the samples, although ST1–ST3 contain comparatively

Table 2 Summary of the XRF analysis results for major elements as oxides (weight %)

Sample	Na$_2$O	MgO	Al$_2$O$_3$	SiO$_2$	P$_2$O$_5$	K$_2$O	CaO	TiO$_2$	MnO	Fe$_2$O$_3$
C1	0.39	0.59	7.23	90.09	0.05	0.04	0.09	0	0	0.44
C2	0.1	<0.008	1.08	97.65	<0.001	0.02	0.06	0.02	0	0.04
C3	0.39	0.59	7.2	89.74	0.05	0.06	0.04	0.01	0	0.5
C4	0.45	0.59	7.19	89.53	0.05	0.05	0.06	0.01	0	0.36
C5	0.47	0.59	7.27	89.47	0.05	0.04	0.12	0	0	0.42
C6	<0.02	<0.008	0.61	97.34	0.02	0.04	0.4	0.01	0	0.03
C7	<0.02	<0.008	0.39	95.8	0.1	0.02	1.51	0.01	0	0.04
C8	<0.02	<0.008	0.25	98.21	<0.001	0.02	0.04	0.01	0	0.05
ST1	0.36	0.5	6.41	79.32	0.04	0.78	1.22	0.19	0.05	5.25
ST2	0.34	0.52	6.48	80.26	0.04	0.46	4.02	0.1	0.06	1.58
ST3	0.14	0.32	3.7	86.33	0.06	0.93	0.22	0.17	0.04	4.32

Table 3 Summary of the XRF analysis results for minor elements (ppm)

| Sample	Cl	V	Cr	Co	Ni	Cu	Zn	As	Se	Rb	Sr	Y	Zr	Nb	Mo	Cd	Sn	Ba	La	Hf	Ta	W	Pb	Th	U
C1	126.3	1.2	981.7	24.7	51.5	17	6.8	3.8	0.2	2.3	14	3.9	0.2	1.5	15	1.4	7.4	<2.0	<2.0	<1.0	9.4	<1.0	<1.0	<1.0	10.6
C2	32	<1.0	31	59	51	4	3	1	1	1	3	6	1	<0.1	<0.3	<2.0	11	<2.0	<2.0	<1.0	7	424	<1.0	<1.0	2
C3	22	9.8	1224	38.6	29.1	27.8	10.9	8.3	0.1	4.4	20.8	21.4	1.3	1.1	18	<2.0	19.4	<2.0	182	<1.0	4	<1.0	<1.0	<1.0	23.4
C4	35.7	1.6	1591	17.9	101.1	26.9	14.7	4.8	0.1	3.9	22.5	15.6	5.9	0.8	18	2.8	25.6	<2.0	<2.0	<1.0	61.1	<1.0	<1.0	<1.0	16
C5	61	11.5	1441	31.7	25.3	33.9	8	5	0.2	2.5	25.4	12.1	2.7	1.3	<1.0	<2.0	19	<2.0	<2.0	<1.0	<1.0	<1.0	<1.0	<1.0	4.9
C6	31	<1.0	29	54	33	7	3	1	1	1	10	5	2	<1.0	<0.3	0	3	4	<2.0	<1.0	5	467	<1.0	<1.0	1
C7	30	3	35	43	42	6	3	1	0	0	37	4	1	<1.0	<0.6	0	8	<2.0	48	<1.0	5	324	<1.0	<1.0	3
C8	9	1	24	47	2	5	2	1	1	0	3	2	1	<1.0	<0.2	0	10	1	<2.0	<1.0	5	397	<1.0	<1.0	2
ST1	262.2	111.5	516.7	66.5	128.7	158.4	147.5	5	0.1	93.8	675.8	180.6	120.4	5.1	10	0.2	<3.0	238	131	8.6	9.8	<1.0	27.2	<1.0	<1.0
ST2	160.2	88.4	641.1	84.5	196.9	45.8	115	57.9	0.1	63.6	1079	153.8	110.2	3.3	<1.0	1.1	12.8	580	112	4.7	102.7	<1.0	25.6	<1.0	<0.8
ST3	64	34	17	36	17	6	54	2	0	34	296	44	33	1	<1.0	0	3	71	44	2	4	206	6	<1.0	0
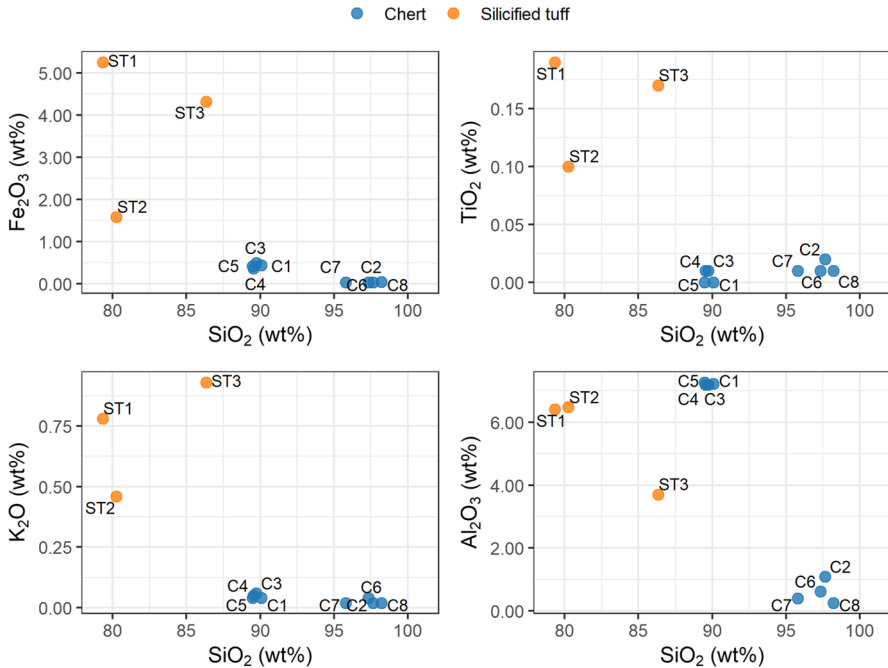
Fig. 8 The relationship between SiO_2 (%) and other major elements among the raw material samples. Figure produced using the R statistical software (R Core Team, [60])

more K_2O, TiO_2, and MnO than does C1–C8 (Fig. 8). In C1–C8, variation in SiO_2 correlates with concentrations of Al_2O_3. As shown in Fig. 8, the four samples that have ~90% SiO_2 (C1, C3, C4, C5) contain the highest amounts of Al_2O_3 among all of the samples analysed (7.19–7.27%), while the other four samples that have > 95% SiO_2 (C2, C6, C7, C8) contain much lower Al_2O_3 (0.25–1.08%). In terms of the trace elements, there is a negative correlation across all of the samples between SiO_2 and Zr (Kendall's tau = − 0.71, $p = 0.003$), Rb (Kendall's tau = − 0.80, $p < 0.001$), Sr (Kendall's tau = − 0.81, $p < 0.001$), Zn (Kendall's tau = − 0.90, $p < 0.001$), Y (Kendall's tau = − 0.67, $p = 0.003$) and Cl (Kendall's tau = − 0.64, $p = 0.006$) (Fig. 9).

Density, Rebound Hardness, and Indentation Hardness

Table 4 summarises the mechanical properties of the raw material samples. Overall, ST1–ST3 exhibit a higher density than that of C1–C8 (p-value 95% confidence interval: 0.015–0.018), which may reflect the higher Fe_2O_3 concentrations among ST1–ST3. However, according to the bootstrapped Mann–Whitney U test, the null hypotheses that rebound hardness (p-value 95% confidence interval: 0.016–0.99) and indentation hardness (p-value 95% confidence interval: 0.016–0.60) are the same in these two samples are not rejected. Instead, the rebound hardness values for all of the samples fall within the upper range associated with chert reported by
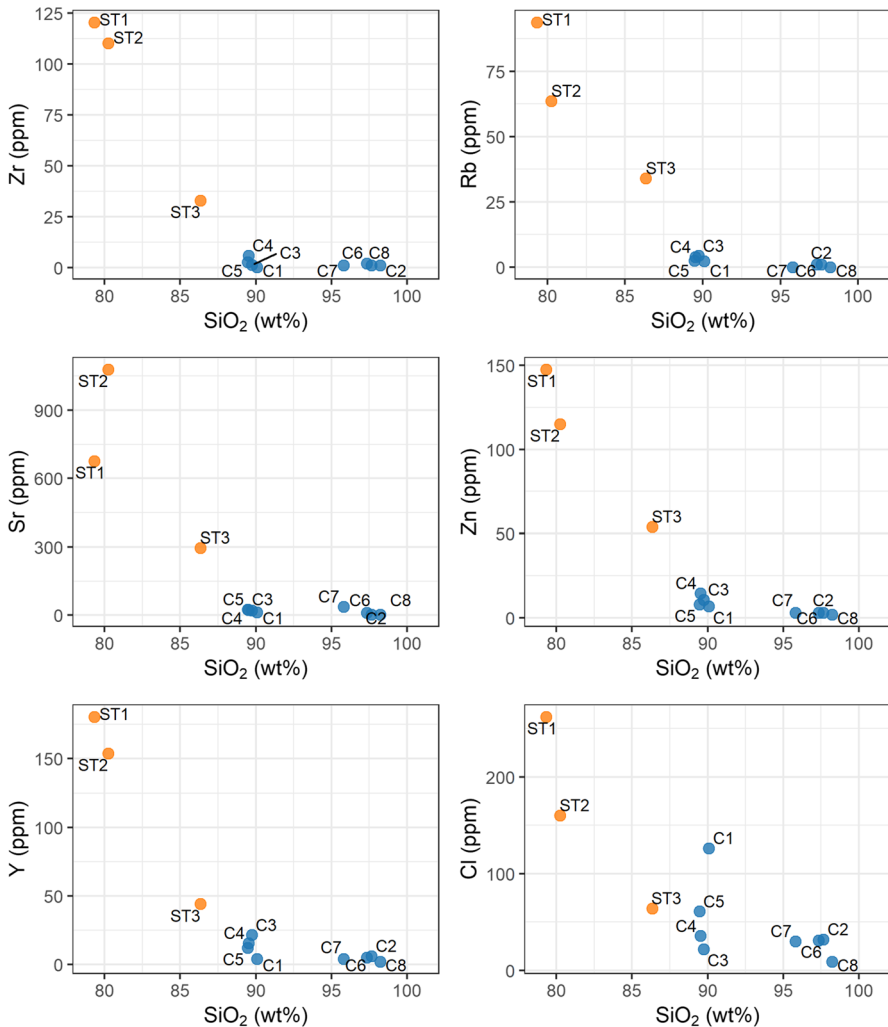
Fig. 9 The relationship between SiO_2 (%) and trace elements among the raw material samples. Figure produced using the R statistical software (R Core Team, [60])

previous studies (Zhou et al., [79]). In contrast, the indentation hardness values observed among our samples are overall notably lower than the published data for chert from elsewhere (8.4–12.1 HK from Namen et al. ([52])).

There is limited evidence that the average HLD and HK values among the samples are correlated (Kendal's tau$=0.45$, $p=0.06$). This finding suggests that the mechanical properties captured by the two measures (i.e. stiffness and plastic deformation resistance) are, at least in part, independent of each other. There is also no evidence that the hardness variation is associated with the difference in SiO_2 concentrations ($SiO_2\%$ vs. HLD: Kendal's tau$=0.38$, $p=0.12$; $SiO_2\%$ vs. HK: Kendal's

Table 4　Summary of the mechanical properties	Sample	Density (g/cm^3)	Leeb rebound hardness (HLD)	Knoop indentation hardness (HK)
	C1	2.42	908.9 ± 20.4	3.54 ± 0.40
	C2	2.43	940.5 ± 12.0	3.99 ± 0.29
	C3	2.22	913.9 ± 7.1	2.61 ± 0.16
	C4	2.35	956.0 ± 5.2	4.29 ± 0.24
	C5	2.46	935.0 ± 14.4	4.62 ± 0.27
	C6	2.40	935.3 ± 17.0	3.92 ± 0.24
	C7	2.32	938.4 ± 6.3	3.54 ± 0.40
	C8	2.38	936.6 ± 19.5	3.36 ± 0.29
	ST1	2.56	905.9 ± 10.1	2.69 ± 0.21
	ST2	2.55	935.9 ± 10.0	3.31 ± 0.34
	ST3	2.56	906.9 ± 11.1	3.06 ± 0.15

tau $= 0.2$, $p = 0.45$). Unfortunately, we were unable to follow Namen et al. ([52]) in using the modified Knoop hardness formula developed by Ben Ghorbal et al. ([5]) to determine the elastic modulus of our samples, as the length of indent impression along the short axis on many of the tested samples cannot be reliably observed (Fig. 10).

Discussion

In this study, we carried out the first geological, mechanical, and quantitative assessment of the two raw materials that dominate the stone artefact assemblages at Liang Bua, described in previous studies as 'chert' and 'silicified tuff' (Moore et al., [46]; Sutikna et al., [67]). Our observations show that both stone types are very similar mineralogically, composed primarily of a very fine-grained quartz matrix supporting abundant foraminifera and algal fossils that have been replaced by silica. There are also instances of quartz crystals and veinlets produced by secondary SiO_2 mineralization that filled existing pore space and/or replaced primary materials. For the 'silicified tuff', no evidence of tuff or other volcanic materials was observed among the samples (ST1–ST3). Instead, geologically both the 'chert' and the 'silicified tuff' derive from limestone that has undergone diagenetic alterations by secondary silica replacement of primary carbonate materials.

The diagenetic process of silica replacement, or silicification, occurs when water within the pore space of carbonate rocks becomes supersaturated with silica, leading to the precipitation of silica and the growth of quartz crystals (Maliva & Siever, [39]). This crystallization, in turn, increases the solubility of the surrounding carbonate minerals and results in further carbonate dissolution and silica recrystallization (Maliva & Siever, [39]). The outcome of this process is the formation of nodular chert, which often occurs in subspherioid, tabular, or irregular forms within carbonate rocks, and can contain partly or wholly silicified remains of calcareous fossils and algal structures (Blatt & Tracy, [6]; Boggs, [7]; Maliva & Siever, [39]),
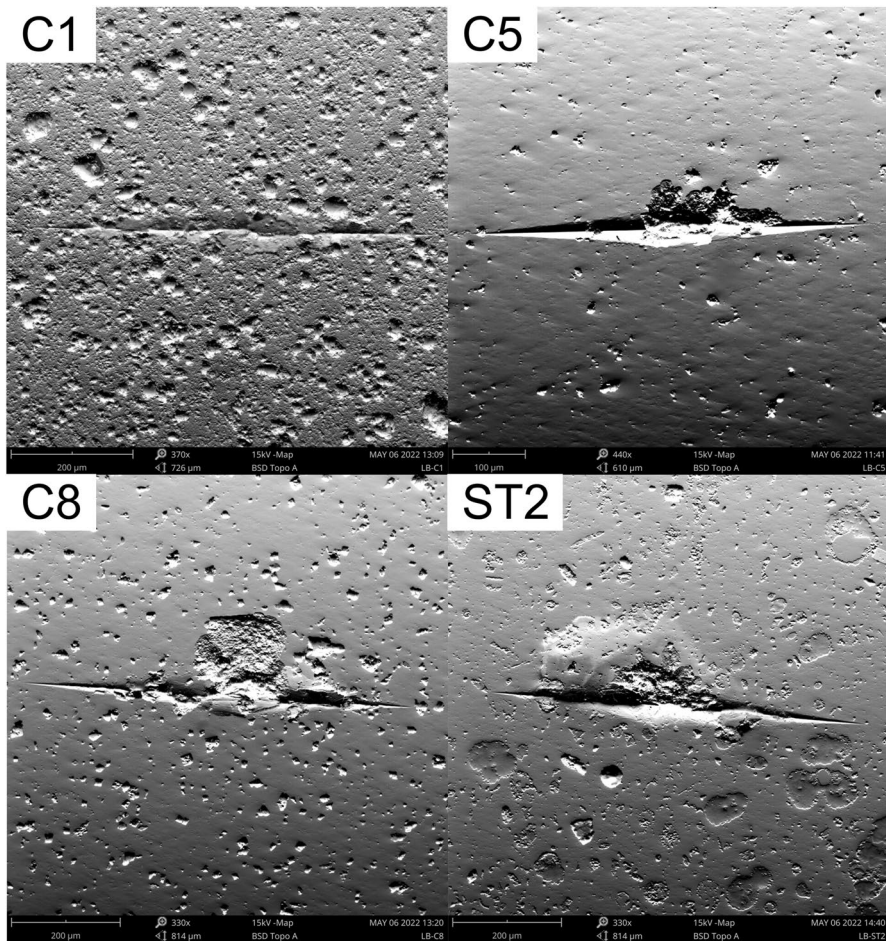
Fig. 10 Examples of the Knoop indentation imprint on the raw material samples. Note how the shorter axis of these indentations cannot be reliably discerned. Images taken using the Phenom XL scanning electron microscope at the University of Wollongong. Figure produced using Inkscape (Inkscape Project, [26])

such as those observed among the samples examined in this study. Note that nodular chert is distinctly different from bedded chert, which develops through the recrystallization of silica from siliceous ooze on ocean floors in the form of bands or layers (Boggs, [7]). In contrast, nodular chert in limestone deposits occurs in a wide variety of environments, ranging from tidal flats to deep ocean basins, with the presence of abundant siliceous sponge spicules in sediments acting as the main control over the silicification process (Maliva & Siever, [39]). Thus, the original formation of the wide variety of limestone-derived materials (i.e., chert) represented at Liang Bua was not necessarily associated with a marine setting exclusively.

From a purely geological perspective, our results suggest that the stone raw materials previously described at Liang Bua as 'chert' and the 'silicified tuff' actually represent different varieties of nodular chert. However, despite this general geological similarity, there are clear geochemical differences between the samples of these two varieties. For instance, the XRF results show that C1–C8 contained higher concentrations of SiO_2, whereas ST1–ST3 consistently yielded greater amounts of Fe_2O_3, TiO_2, and K_2O, as well as trace elements such as Zr, Rb, and Zn. The more elevated concentrations of Fe_2O_3 among ST1–ST3 ($> 1\%$) may also help to explain their notable colour variation (pale/greyish green to brown) and higher density values compared with those of C1–C8. Therefore, the 'chert' and 'silicified tuff' categories used in previous studies are more aptly described as silica-dominated (i.e. SiO_2-dominated) nodular chert and iron-rich (i.e. Fe_2O_3-rich) nodular chert, respectively, at least based on the examination of samples used in this study (C1–C8 and ST1–ST3).

The geochemical differences that we observed between the iron-rich samples (ST1–ST3) and the silica-dominated samples (C1–C8) may reflect relative dilution of the various elements through the silicification process. Indeed, several major and trace elements, including Fe_2O_3, Zr, Rb, Sr, Zn, Y, and Cl, correlate negatively with SiO_2 among the entire combined sample (Figs. 8 and 9). In particular, the negative relationship between Zr and SiO_2 must be related to the enrichment of SiO_2 rather than the diagenetic loss of Zr, because Zr is immobile. If this hypothesis is correct, it suggests that the observed variation among the two sample groups examined here simply reflects respective differences in the extent of diagenetic alteration on similar primary materials derived from single geological settings. However, there are indications that the two raw material groups might be derived from different geological formations, as the iron-rich nodular chert (previously described as 'silicified tuff') only appears to occur as alluvial material in the riverbed and not in the surrounding limestone hills. Thus, it makes sense that the source of this raw material is located farther upstream to the south, closer to the modern town of Ruteng. This town is situated in the Kiro Formation, which is composed primarily of a Miocene volcanic sequence (Koesoemadinata et al., [34]). This hypothesis predicts that the largely volcanic rocks farther upstream from Liang Bua must also contain some limestone beds in which silicification took place to produce the highly siliceous yet iron-rich stones. The volcanic environment may also help explain the occurrence of the coarser, clast-supported matrix observed in some of the iron-rich samples, which may be related to volcaniclastic units that went through secondary silicification.

For the silica-dominated nodular chert (previously described as 'chert'), on the other hand, our survey recovered samples only at localised outcrops among the limestone hills around Liang Bua, and not in the river cobble bed. These chert nodules likely represent products of silicification within the local Waihekang Formation, which has been noted to contain thick limestone beds with fragments of chert and unspecified fossils (Westaway et al., [73]). In this case, the geochemical variation observed among C1–C8, such as in SiO_2 and Al_2O_3 (Fig. 6), could reflect differences in the silicification process and/or post-depositional weathering. For example, a previous study has shown that weathered chert artefacts can

contain higher concentrations of aluminium under certain soil conditions (Sheppard & Pavlish, [64]). This is because the solubility of silica and aluminium varies by soil pH, such that under certain conditions silica can be dissolved and removed at a higher rate than with aluminium, which in turn causes aluminium to become enriched relative to SiO_2 (Sheppard & Pavlish, [64]). Thus, the samples examined here that contain relatively lower SiO_2 and higher Al_2O_3 (C1, C3, C4, and C5) might represent the more weathered version of the silica-dominated nodular chert that occurs around Liang Bua.

It is important to establish the geological characteristics of these two varieties of nodular chert because the Liang Bua stone artefact sequence suggests a shift in the way past people acquired lithic raw materials for stone tool production at the site. As outlined above, the lithic assemblage associated with *H. floresiensis* largely consists of artefacts made using the iron-rich nodular chert (70%) (Sutikna et al., [67]; also see Moore et al., [46]), which seems to only occur in the Wae Racang today according to our opportunistic survey. From ~ 46 ka until the Holocene, however, the percentage of artefacts made from the iron-rich variety declined considerably (34%), while the silica-dominated variety with chalky cortex became more commonly used (45%). As Sutikna et al. ([67]) noted, the simplest hypothesis for this shift in raw material representation is that after ~ 46 ka, the silica-dominated chert became more widely available around Liang Bua than it had been previously, possibly due to erosion and downcutting that exposed previously buried outcrops among the limestone hills. However, Sutikna et al. ([67]) contended that this scenario is unlikely given that the iron-rich chert variety occurring in the river remains the most abundant and easily accessible material in the region today. Instead, it was proposed that the shift in raw material usage may reflect a greater reliance by *H. floresiensis* on stones readily available in the adjacent Wae Racang, while the modern human populations that used the cave after ~ 46 ka selectively transported preferred raw materials (i.e. the silica-dominated chert) from farther away (Moore et al., [46]; Sutikna et al., [67]). However, our survey showed that the silica-dominated chert is also equally available in the vicinity of the cave (500–700 m), meaning that the increased discard of this raw material does not necessarily imply a greater degree of its transport from distant sources. Instead, the evidence suggests that, assuming both raw material types were available locally as today, modern humans simply acquired the silica-dominated raw material more frequently than did *H. floresiensis*.

If modern humans preferentially procured the silica-dominated chert over the iron-rich variety, it is unlikely that this preference was related to fracture predictability. All of the raw material samples analysed in this study show very fine-grained matrices and high SiO_2 concentrations. Moreover, there was no detectable dissimilarity in the rebound hardness between the two chert types and all of the observed measurements are comparable to values reported for chert by previous studies (Zhou et al., [79]). Thus, if rebound hardness is used as a proxy for raw material homogeneity and fracture predictability (Braun et al., [10]; Egeland et al., [18]; Noll, [55]), then there is no reason to suspect that these two raw material varieties share any major differences in flaking quality.

An alternative hypothesis is that the raw material shift at Liang Bua was related to the sharpness and durability of tool edges during tool use activities. The ability of a

stone to resist abrasion and plastic deformation has been shown to correlate directly with the stone's rebound and indentation hardness (Çelik & Çobanoğlu, [17]; Erickson et al., [19]). However, as with rebound hardness, there was no detectable difference in the indentation hardness of the two raw material groups examined here, suggesting that the tool edge produced from the two stone types may share similar functional attributes, such as edge durability. However, it is important to note that the sample size used in this study is small and our observations need to be verified by future studies with more samples. In addition, further studies should evaluate the functional hypothesis by testing directly the quality and performance of flake edges made from the two chert varieties under controlled tool-use settings (Calandra et al., [16]; Key, [32]; Key et al., [33]; Lin et al., [38]). Another interesting finding here is that the indentation hardness of all of our samples is considerably lower than those of chert from elsewhere (Namen et al., [52]). This outcome demonstrates that geologically similar stone types can have markedly different mechanical properties, and these differences would likely have influenced the selection and transport of lithic raw materials in the past. Therefore, it is important for lithic raw material studies to look beyond general geological classifications (and their assumed 'good' versus 'bad' qualities for stone tool technology) and quantitatively characterise attributes related to their knappability and functional performance.

If the two chert varieties at Liang Bua share similar mechanical properties, it is possible that the increased utilisation of the silica-dominated variety by *H. sapiens* at the site was related more to socio-cultural factors. Indeed, adzes made from the same material were commonly associated with late Holocene burials in the region (Moore et al., [46]), suggesting that the raw material was connected to social attributes such as prestige and status signaling. It is therefore possible that the use of the silica-dominated chert by earlier modern humans was conditioned by similar social processes. Be that as it may, explanations referring to social factors are difficult to test. Moreover, there are other ecological factors that could potentially explain the shifts in the dominant raw material varieties at Liang Bua. For instance, it has been established that forager movement and toolkit curation can directly affect the spatial patterning of lithic raw materials on the archaeological landscape (Brantingham, [8]; Lin & Premo, [37]; White, [74]). Depending on the distribution of the raw material sources (Oestmo et al., [56]; Pop, [57]), more expansive forager land use through longer movement distances may cause stone artefacts to be discarded farther away from raw material sources. Similarly, higher degrees of toolkit curation and maintenance can also result in the disposal of more artefacts at greater distances away from source (Lin & Premo, [37]). Even if the two primary chert varieties represented at Liang Bua are available in the local area, variation in their spatial distribution and availability on the landscape alone (river versus localised inland sources) could influence their respective uptake by past hominins. For instance, if modern humans had a greater foraging range and/or relied more on logically organised mobility than *H. floresiensis*, then it may be possible that modern human foragers at Liang Bua encountered and hence procured the silica-dominated chert from inland sources more frequently. If this was the case, the increased proportion of the silica-dominated chert discarded at Liang Bua after ~ 46 ka could signal changes in broader processes such as foraging range, movement distance, and/or technological

organization. To empirically verify this hypothesis, it is necessary to conduct more systematic raw material survey and sampling at a larger scale to adequately summarise the distribution of different lithic raw materials across the landscape around Liang Bua. Moreover, it is necessary to unpack the various mobility and land use scenarios to examine how each of these processes affect the accumulation of lithic discards on archaeological landscapes (Lin and Premo, [37]; White, [74]). To this end, a promising approach is to combine formal spatial modelling with more comprehensive raw material sourcing information (e.g., Pop et al., [58]) and ecological data (Veatch et al., [80]) to test if specific forager procurement and mobility scenarios generate patterns of raw material discard proportions similar to those observed at Liang Bua without targeted selection of particular stone types. Such studies may provide further critical insights into the comparative behaviours of *H. sapiens* and *H. floresiensis*.

Conclusion

To date, geological details about the two dominant lithic raw materials at Liang Bua have been limited to qualitative observations and descriptions. This study is the first systematic effort to quantitatively characterise the geological and mechanical properties of these raw materials. Our results show that the two major stone types at the site, referred to in previous studies as 'chert' and 'silicified tuff' (Moore et al., [46]; Sutikna et al., [67]), are in fact similar in their geological and mineralogical structures and represent varieties of nodular chert formed through diagenetic silica replacement in carbonate rocks. However, these two raw material varieties differ from one another in several geochemical features. These differences, such as the concentration of Fe_2O_3, help explain disparities between the two stone types that have been noted in previous studies (e.g., differences in colour and density). As such, we proposed that the 'chert' and 'silicified tuff' at Liang Bua are more aptly described respectively as silica-dominated (i.e. SiO_2-dominated) nodular chert and iron-rich (i.e. Fe_2O_3-rich) nodular chert. In contrast to the geochemical variation, no difference was observed between these two raw materials in their hardness properties, suggesting limited variation in their knappability and tool edge functional quality, such as durability. Instead, the observed shift in raw material utilisation at Liang Bua that occurred after~46 ka may be related to factors beyond tool manufacture and function. To further explore these hypotheses, larger scale systematic sampling is needed to better characterise the raw material distribution across the Liang Bua landscape, which can in turn be integrated into formal models of hominin raw material procurement and land use.

Data Availability The datasets generated and analysed by the current study are available in the Zenodo repository, https://doi.org/10.5281/zenodo.7145681.

Declarations

References

1. Abrunhosa, A., Pereira, T., Márquez, B., Baquedano, E., Arsuaga, J. L., & Pérez-González, A. (2019). Understanding Neanderthal technological adaptation at Navalmaíllo Rock Shelter (Spain) by measuring lithic raw materials performance variability. *Archaeological and Anthropological Sciences, 11*, 5949–5962. https://doi.org/10.1007/s12520-019-00826-3

2. Aldeeky, H., Al Hattamleh, O., & Rababah, S. (2020). Assessing the uniaxial compressive strength and tangent Young's modulus of basalt rock using the Leeb rebound hardness test. *Materiales De Construcción, 70*(340), e230. https://doi.org/10.3989/MC.2020.15119

3. Andrefsky, W. (1994). Raw-material availability and the organization of technology. *American Antiquity, 59*(1), 21–34. https://doi.org/10.2307/3085499

4. Banning, E. B. (2021). Sampled to death? The rise and fall of probability sampling in archaeology. *American Antiquity, 86*(1), 43–60. https://doi.org/10.1017/aaq.2020.39

5. Ben Ghorbal, G., Tricoteaux, A., Thuault, A., Louis, G., & Chicot, D. (2017). Comparison of conventional Knoop and Vickers hardness of ceramic materials. *Journal of the European Ceramic Society, 37*(6), 2531–2535. https://doi.org/10.1016/j.jeurceramsoc.2017.02.014

6. Blatt, H., & Tracy, R. (1996). *Petrology: Igneous, sedimentary, and metamorphic*. Freeman.

7. Boggs, S. J. (2009). *Petrology of sedimentary rocks*. Cambridge University Press.

8. Brantingham, P. J. (2006). Measuring forager mobility. *Current Anthropology, 47*(3), 435–459. https://doi.org/10.1086/503062

9. Brantingham, P. J., Olsen, J. W., Rech, J. A., & Krivoshapkin, A. I. (2000). Raw material quality and prepared core technologies in Northeast Asia. *Journal of Archaeological Science, 27*(3), 255–271. https://doi.org/10.1006/jasc.1999.0456

10. Braun, D. R., Plummer, T., Ferraro, J. V., Ditchfield, P., & Bishop, L. C. (2009). Raw material quality and Oldowan hominin toolstone preferences: Evidence from Kanjera South. *Kenya. Journal of Archaeological Science, 36*(7), 1605–1614. https://doi.org/10.1016/j.jas.2009.03.025

11. Brown, P., & Maeda, T. (2009). Liang Bua *Homo floresiensis* mandibles and mandibular teeth: A contribution to the comparative morphology of a new hominin species. *Journal of Human Evolution, 57*(5), 571–596. https://doi.org/10.1016/j.jhevol.2009.06.002

12. Brown, P., Sutikna, T., Morwood, M. J., Soejono, R. P., Jatmiko, W. S., & E., & Rokus Awe Due,. (2004). A new small-bodied hominin from the Late Pleistocene of Flores, Indonesia. *Nature, 431*, 1055–1061. https://doi.org/10.1038/nature02999

13. Brumm, A., Aziz, F., van den Bergh, G. D., Morwood, M. J., Moore, M. W., Kurniawan, I., Hobbs, D. R., & Fullagar, R. (2006). Early stone technology on Flores and its implications for *Homo floresiensis*. *Nature, 441*, 624–628. https://doi.org/10.1038/nature04618

14. Brumm, A., Jensen, G. M., van den Bergh, G. D., Morwood, M. J., Kurniawan, I., Aziz, F., & Storey, M. (2010). Hominins on Flores, Indonesia, by one million years ago. *Nature, 464*, 748–752. https://doi.org/10.1038/nature08844

15. Brumm, A., van den Bergh, G. D., Storey, M., Kurniawan, I., Alloway, B. V., Setiawan, R., Setiyabudi, E., Grün, R., Moore, M. W., Yurnaldi, D., Puspaningrum, M. R., Wibowo, U. P., Insani, H., Sutisna, I., Westgate, J. A., Pearce, N. J. G., Duval, M., Meijer, H. J. M., Aziz, F., … Morwood, M. J. (2016). Age and context of the oldest known hominin fossils from Flores. *Nature, 534*, 249–253. https://doi.org/10.1038/nature17663

16. Calandra, I., Gneisinger, W., & Marreiros, J. (2020). A versatile mechanized setup for controlled experiments in archeology. STAR: Science & Technology of Archaeological Research, 6, 30–40. https://doi.org/10.1080/20548923.2020.1757899

17. Çelik, S. B., & Çobanoğlu, İ. (2019). Comparative investigation of Shore, Schmidt, and Leeb hardness tests in the characterization of rock materials. *Environmental Earth Sciences, 78*, 554. https://doi.org/10.1007/s12665-019-8567-7

18. Egeland, C. P., Fadem, C. M., Byerly, R. M., Henderson, C., Fitzgerald, C., Mabulla, A. Z., Baquedano, E., & Gidna, A. (2019). Geochemical and physical characterization of lithic raw materials in the Olduvai Basin, Tanzania. *Quaternary International, 526*, 99–115. https://doi.org/10.1016/j.quaint.2019.09.036

19. Erickson, L. C., Hawthorne, H. M., & Troczynski, T. (2001). Correlations between microstructural parameters, micromechanical properties and wear resistance of plasma sprayed ceramic coatings. *Wear, 250*(1–12), 569–575. https://doi.org/10.1016/S0043-1648(01)00608-1

20. Falk, D., Hildebolt, C., Smith, K., Morwood, M. J., Sutikna, T., Brown, P., Jatmiko, W. S., & E., Brunsden, B., & Prior, F. (2005). The brain of LB1, *Homo floresiensis*. *Science, 308*(5719), 242–245. https://doi.org/10.1126/science.1109727

21. Gauthier, G., Burke, A. L., & Leclerc, M. (2012). Assessing XRF for the geochemical characterization of radiolarian chert artifacts from northeastern North America. *Journal of Archaeological Science, 39*(7), 2436–2451. https://doi.org/10.1016/j.jas.2012.02.019

22. Grave, P., Attenbrow, V., Sutherland, L., Pogson, R., & Forster, N. (2012). Non-destructive pXRF of mafic stone tools. *Journal of Archaeological Science, 39*(6), 1674–1686. https://doi.org/10.1016/j.jas.2011.11.011

23. Hall, G. E. M., Bonham-Carter, G. F., & Buchar, A. (2014). Evaluation of portable X-ray fluorescence (pXRF) in exploration and mining: Phase 1, control reference materials. *Geochemistry: Exploration. Environment, Analysis, 14*, 99–123. https://doi.org/10.1144/geochem2013-241

24. Harahap, B. H., Abidin, H. Z., Utoyo, H., Djumhana, D., & Yuniarni, R. (2015). Prospect of mineral deposits in the central Flores Island, Eastern Indonesia. *Jurnal Geologi Dan Sumberdaya Mineral, 16*(1), 1–13.

25. Hayes, E., Fullagar, R., Kamminga, J., Prinsloo, L. C., Bordes, L., Sutikna, T., Tocheri, M. W., Wahyu Saptomo, E., Jatmiko, & Roberts, R. G. (2021). Use-polished stone flakes from Liang Bua, Indonesia: Implications for plant processing and fibrecraft in the Late Pleistocene. Journal of Archaeological Science: Reports, 40(A), 103199. https://doi.org/10.1016/j.jasrep.2021.103199

26. Inkscape Project (2020). Inkscape. https://inkscape.org

27. Jungers, W. L., Harcourt-Smith, W. E., Wunderlich, R. E., Tocheri, M. W., Larson, S. G., Sutikna, T., Due, R. A., & Morwood, M. J. (2009a). The foot of *Homo floresiensis*. *Nature, 459*, 81–84. https://doi.org/10.1038/nature07989

28. Jungers, W. L., Larson, S. G., Harcourt-Smith, W., Morwood, M. J., Sutikna, T., Due, R. A., & Djubiantono, T. (2009b). Descriptions of the lower limb skeleton of *Homo floresiensis*. *Journal of Human Evolution, 57*(5), 538–554. https://doi.org/10.1016/j.jhevol.2008.08.014

29. Kaifu, Y., Baba, H., Sutikna, T., Morwood, M. J., Kubo, D., Wahyu Saptomo, E., & JatmikoDue, & Djubiantono, T., R. A. (2011). Craniofacial morphology of *Homo floresiensis*: Description, taxonomic affinities, and evolutionary implication. *Journal of Human Evolution, 61*(6), 644–682.

30. Kaifu, Y., Kono, R. T., Sutikna, T., Wahyu Saptomo, E., & Due, R. A. (2015a). Unique dental morphology of *Homo floresiensis* and its evolutionary implications. *PLoS ONE, 10*(11), e0141614.

31. Kaifu, Y., Kono, R. T., Sutikna, T., Wahyu Saptomo, E., Due, R. A., & Baba, H. (2015b). Descriptions of the dental remains of *Homo floresiensis*. *Anthropological Science, 123*(2), 129–145. https://doi.org/10.1537/ase.150501

32. Key, A. J. M. (2016). Integrating mechanical and ergonomic research within functional and morphological analyses of lithic cutting technology: Key principles and future experimental directions. *Ethnoarchaeology, 8*(1), 69–89. https://doi.org/10.1080/19442890.2016.1150626

33. Key, A., Proffitt, T., & de la Torre, I. (2020). Raw material optimization and stone tool engineering in the Early Stone Age of Olduvai Gorge (Tanzania). *Journal of the Royal Society Interface, 17*(162), 20190377. https://doi.org/10.1098/rsif.2019.0377

34. Koesoemadinata, S., Noya, Y., & Kadarisman, D. (1994). Geological map of the Ruteng Quadrangle, Nusa Tenggara, scale 1:250,000. *Geological Research and Development Center, Indonesia.*

35. Larson, S. G., Jungers, W. L., Tocheri, M. W., Orr, C. M., Morwood, M. J., Sutikna, T., Awe, R. D., & Djubiantono, T. (2009). Descriptions of the upper limb skeleton of *Homo floresiensis*. *Journal of Human Evolution, 57*(5), 555–570. https://doi.org/10.1016/j.jhevol.2008.06.007

36. Lemorini, C., Bishop, L. C., Plummer, T. W., Braun, D. R., Ditchfield, P. W., & Oliver, J. S. (2019). Old stones' song—Second verse: Use-wear analysis of rhyolite and fenetized andesite artifacts from the Old-owan lithic industry of Kanjera South, Kenya. *Archaeological and Anthropological Sciences, 11*, 4729–4754. https://doi.org/10.1007/s12520-019-00800-z

37. Lin, S. C., & Premo, L. S. (2021). Forager mobility and lithic discard probability similarly affect the distance of raw material discard from source. *American Antiquity, 86*(4), 845–863. https://doi.org/10.1017/aaq.2021.66

38. Lin, S. C., Rezek, Z., & Dibble, H. L. (2018). Experimental design and experimental inference in stone arti-fact archaeology. *Journal of Archaeological Method and Theory, 25*(3), 663–688. https://doi.org/10.1007/s10816-017-9351-1

39. Maliva, R. G., & Siever, R. (1989). Nodular chert formation in carbonate rocks. *The Journal of Geology, 97*(4), 421–433. https://doi.org/10.1086/629320

40. Malyk-Selivanova, N., Ashley, G. M., Gal, R., Glascock, M. D., & Neff, H. (1998). Geological–geochemi-cal approach to "sourcing" of prehistoric chert artifacts, northwestern Alaska. *Geoarchaeology, 13*(7), 673–708. https://doi.org/10.1002/(SICI)1520-6548(199810)13:7%3c673::AID-GEA2%3e3.0.CO;2-3

41. Marwick, B., Clarkson, C., O'Connor, S., & Collins, S. (2016). Early modern human lithic technology from Jerimalai, East Timor. *Journal of Human Evolution, 101*, 45–64. https://doi.org/10.1016/j.jhevol.2016.09.004

42. McPherron, S. P., Braun, D. R., Dogandžić, T., Archer, W., Desta, D., & Lin, S. C. (2014). An experimental assessment of the influences on edge damage to lithic artifacts: A consideration of edge angle, substrate grain size, raw material properties, and exposed face. *Journal of Archaeological Science, 49*, 70–82. https://doi.org/10.1016/j.jas.2014.04.003

43. Moore, M. W. (2007). Lithic design space modelling and cognition in *Homo floresiensis*. In A. C., Schalley, & D. Khlentzos (Eds.), *Mental stages, volume 1: Evolution, function, and nature* (pp. 11–34). John Benja-mins Publishing Company

44. Moore, M. W., & Brumm, A. (2007). Stone artifacts and hominins in island Southeast Asia: New insights from Flores, eastern Indonesia. *Journal of Human Evolution, 52*(1), 85–102. https://doi.org/10.1016/j.jhevol.2006.08.002

45. Moore, M. W., & Brumm, A. (2009). *Homo floresiensis* and the African Oldowan. In E. Hovers & D. R. Braun (Eds.), *Interdisciplinary approaches to the Oldowan: Vertebrate paleobiology and paleoanthropol-ogy* (pp. 61–69). Springer. https://doi.org/10.1007/978-1-4020-9060-8

46. Moore, M. W., Sutikna, T., Jatmiko, M., & M. J., & Brumm, A. (2009). Continuities in stone flaking tech-nology at Liang Bua, Flores. *Indonesia. Journal of Human Evolution, 57*(5), 503–526. https://doi.org/10.1016/j.jhevol.2008.10.006

47. Morley, M. W., Goldberg, P., Sutikna, T., Tocheri, M. W., Prinsloo, L. C., Jatmiko, W. S., & E., Wasisto, S., & Roberts, R. G. (2017). Initial micromorphological results from Liang Bua, Flores (Indonesia): Site forma-tion processes and hominin activities at the type locality of *Homo floresiensis*. *Journal of Archaeological Science, 77*, 125–142. https://doi.org/10.1016/j.jas.2016.06.004

48. Morwood, M. J., Brown, P., Jatmiko, S., & T., Wahyu Saptomo, E., Westaway, K. E., Rokus Awe Due, Roberts, R. G., Maeda, T., Wasisto, S., & Djubiantono, T. (2005). Further evidence for small-bodied hominins from the Late Pleistocene of Flores, Indonesia. *Nature, 437*, 1012–1017. https://doi.org/10.1038/nature04022

49. Morwood, M. J., Soejono, R. P., Roberts, R. G., Sutikna, T., Turney, C. S. M., Westaway, K. E., Rink, W. J., Zhao, J. X., van den Bergh, G. D., Due, R. A., Hobbs, D. R., Moore, M. W., Bird, M. I., & Fifield, L. K.

(2004). Archaeology and age of a new hominin from Flores in eastern Indonesia. *Nature, 431*, 1087–1091. https://doi.org/10.1038/nature02956

50. Morwood, M. J., Sutikna, T., Saptomo, E. W., Jatmiko, H., & D. R., & Westaway, K. E. (2009). Preface: Research at Liang Bua, Flores. *Indonesia. Journal of Human Evolution, 57*(5), 437–449. https://doi.org/10.1016/j.jhevol.2009.07.003

51. Murray, R. W. (1994). Chemical criteria to identify the depositional environment of chert: General principles and applications. *Sedimentary Geology, 90*(3–4), 213–232. https://doi.org/10.1016/0037-0738(94)90039-6

52. Namen, A., Iovita, R., Nickel, K. G., Varis, A., Taimagambetov, Z., & Schmidt, P. (2022). Mechanical properties of lithic raw materials from Kazakhstan: Comparing chert, shale, and porphyry. *PLoS ONE, 17*, e0265640.

53. Nanlohy, F., Sitorus, K., Kasbani, D., & S., & Simanjuntak, J. (2002). Subsurface geology of the Mataloko geothermal field deduced from MTL-1, MT-1 and MT-2 wells, central Flores, East Nusa Tenggara, Indonesia. *Bulletin of the Geological Survey of Japan, 53*(2/3), 329–336. https://doi.org/10.9795/bullgsj.53.329

54. Newlander, K., Goodale, N., Jones, G. T., & Bailey, D. G. (2015). Empirical study of the effect of count time on the precision and accuracy of pXRF data. *Journal of Archaeological Science: Reports, 3*, 534–548. https://doi.org/10.1016/j.jasrep.2015.07.007

55. Noll, M. P. (2000). Components of Acheulian lithic assemblage variability at Olorgesailie, Kenya. Unpublished Ph.D. dissertation, University of Illinois at Urbana-Champaign.

56. Oestmo, S., Janssen, M. A. & Marean, C. W. (2016). Testing Brantingham's neutral model: The effect of spatial clustering on stone raw material procurement. In J. A. Barceló, & F. Del Castillo (Eds.), *Simulating prehistoric and ancient worlds* (pp. 175–188). Springer. https://doi.org/10.1007/978-3-319-31481-5_4

57. Pop, C. M. (2016). Simulating lithic raw material variability in archaeological contexts: A re-evaluation and revision of Brantingham's neutral model. *Journal of Archaeological Method and Theory, 23*, 1127–1161. https://doi.org/10.1007/s10816-015-9262-y

58. Pop, C. M., Wilson, L., & Browne, C. L. (2022). Evaluating landscape knowledge and lithic resource selection at the French Middle Paleolithic site of the Bau de l'Aubesier. *Journal of Human Evolution, 166*, 103152. https://doi.org/10.1016/j.jhevol.2022.103152

59. QGIS Development Team (2022). QGIS Geographic Information System. Open Source Geospatial Foundation. http://qgis.org

60. R Core Team (2021). R: A language and environment for statistical computing. R Foundation for Statistical Computing, Vienna, Austria. https://www.R-project.org/.

61. Schneider, C. A., Rasband, W. S., & Eliceiri, K. W. (2012). NIH Image to ImageJ: 25 years of image analysis. *Nature Methods, 9*, 671–675. https://doi.org/10.1038/nmeth.2089

62. Seong, C. (2004). Quartzite and vein quartz as lithic raw materials reconsidered: A view from the Korean paleolithic. *Asian Perspectives, 43*(1), 73–91. https://doi.org/10.1353/asi.2004.0016

63. Sheppard, P. J., Irwin, G. J., Lin, S. C., & McCaffrey, C. P. (2011). Characterization of New Zealand obsidian using PXRF. *Journal of Archaeological Science, 38*(1), 45–56. https://doi.org/10.1016/j.jas.2010.08.007

64. Sheppard, P. J., & Pavlish, L. A. (1992). Weathering of archaeological cherts: A case study from the Solomon Islands. *Geoarchaeology, 7*(1), 41–53. https://doi.org/10.1002/gea.3340070104

65. Sherwood, N., 2019. Analyzing lithic raw material qualities and hominid selectivity in the Early Palaeolithic. Unpublished Ph.D. dissertation, University of the Witwatersrand.

66. Shipton, C., O'Connor, S., Jankowski, N., O'Connor-Veth, J., Maloney, T., Kealy, S., & Boulanger, C. (2019). A new 44,000-year sequence from Asitau Kuru (Jerimalai), Timor-Leste, indicates long-term continuity in human behaviour. *Archaeological and Anthropological Sciences, 11*, 5717–5741. https://doi.org/10.1007/s12520-019-00840-5

67. Sutikna, T., Tocheri, M. W., Faith, J. T., Jatmiko, R. D., Awe, M., & H. J. M., Wahyu Saptomo, E., & Roberts, R. G. (2018). The spatio-temporal distribution of archaeological and faunal finds at Liang Bua (Flores, Indonesia) in light of the revised chronology for *Homo floresiensis*. *Journal of Human Evolution, 124*, 52–74. https://doi.org/10.1016/j.jhevol.2018.07.001

68. Sutikna, T., Tocheri, M. W., Morwood, M. J., Wahyu Saptomo, E., Jatmiko, R. D., Awe, W., & S., Westaway, K. E., Aubert, M., Li, B., Zhao, J. -x., Storey, M., Alloway, B. V., Morley, M. W., Meijer, H. J. M., van den Bergh, G. D., Grün, R., Dosseto, A., Brumm, A., Jungers, W. L., & Roberts, R. G. (2016). Revised stratigraphy and chronology for *Homo floresiensis* at Liang Bua in Indonesia. *Nature, 532*, 366–369. https://doi.org/10.1038/nature17179

69. Tocheri, M. W., Larson, S. G., Sutikna, T., Jatmiko, E., Wahyu Saptomo, E., Due, R. A., Djubiantono, T., Morwood, M. J., & Jungers, W. L. (2007). The primitive wrist of *Homo floresiensis* and its implications for hominin evolution. *Science, 317*, 1743–1745. https://doi.org/10.1126/science.1147143

70. Tocheri, M. W., Veatch, E. G., Jatmiko, Wahyu Saptomo, E., & Sutikna, T. (2022). *Homo floresiensis*. In C. F. W. Higham & N. C. Kim (Eds.), *The Oxford handbook of early Southeast Asia* (pp. 38–69). Oxford University Press. https://doi.org/10.1093/oxfordhb/9780199355358.001.0001

71. Toraya, H. (2016). A new method for quantitative phase analysis using X-ray powder diffraction: Direct derivation of weight fractions from observed integrated intensities and chemical compositions of individual phases. *Journal of Applied Crystallography, 49*, 1508–1516. https://doi.org/10.1107/S1600576716010451

72. Wang, Y., Grammer, G. M., Eberli, G., Weger, R., & Nygaard, R. (2022). Testing rebound hardness for estimating rock properties from core and wireline logs in mudrocks. *Journal of Petroleum Science and Engineering, 210*, 109973. https://doi.org/10.1016/j.petrol.2021.109973

73. Westaway, K. E., Roberts, R. G., Sutikna, T., Morwood, M. J., Drysdale, R., Zhao, J., & x., & Chivas, A.R. (2009). The evolving landscape and climate of western Flores: An environmental context for the archaeological site of Liang Bua. *Journal of Human Evolution, 57*(5), 450–464. https://doi.org/10.1016/j.jhevol.2009.01.007

74. White, A. (2021). Lithic transport patterns, tool curation behavior, and group range estimates: A model-based exploration. *Journal of Computer Applications in Archaeology, 4*(1), 254–273. https://doi.org/10.5334/jcaa.82

75. Yaşar, E., & Erdoğan, Y. (2004). Estimation of rock physicomechanical properties using hardness methods. *Engineering Geology, 71*(3–4), 281–288. https://doi.org/10.1016/S0013-7952(03)00141-8

76. Yonekura, K. (2015). Rock properties and material selection for blade manufacture in upper paleolithic Japan. *Lithic Technology, 40*(2), 85–93. https://doi.org/10.1179/2051618515Y.0000000001

77. Yonekura, K., Hasegawa, H., Hotta, A., & Suzuki, T. (2008). A novel approach to studies of prehistoric exploitation of stone tool materials using material composition, surface morphology, microstructure and mechanical properties. *Archaeometry, 50*(5), 727–746. https://doi.org/10.1111/j.1475-4754.2008.00374.x

78. Yonekura, K., & Suzuki, T. (2009). Microhardness analysis and characterization of Palaeolithic stone tool materials for understanding primary material selections and utilizations. *Materials Characterization, 60*(4), 282–291. https://doi.org/10.1016/j.matchar.2008.08.008

79. Zhou, J., Mandal, S., Chen, F., Quest, M., & Hume, D. (2018). Reservoir geomechanic heterogeneity index (RGHI): Concept, methodology, and application. Paper presented at the SPE/AAPG/SEG Unconventional Resources Technology Conference 2018, Houston. https://doi.org/10.15530/urtec-2018-2902828

80. Veatch, E. G., Tocheri, M. W., Sutikna, T., McGrath, K., Saptomo, E. W., Jatmiko, Helgen, K. M. (2019). Temporal shifts in the distribution of murine rodent body size classes at Liang Bua (Flores Indonesia) reveal new insights into the paleoecology of Homo floresiensis and associated fauna. *Journal of Human Evolution* 13045–60 S0047248418302239 https://doi.org/10.1016/j.jhevol.2019.02.002

Authors and Affiliations

Sam C. Lin[1,2] ⬤ **· Lloyd T. White[3] · Jatmiko[4] · I Made Agus Julianto[5] ·
Matthew W. Tocheri[2,5,6] · Thomas Sutikna[1,2]**

[1]   Centre for Archaeological Science, School of Earth, Atmospheric and Life Sciences, University
     of Wollongong, Wollongong, NSW, Australia

[2]   Australian Research Council Centre of Excellence for Australian Biodiversity and Heritage,
     University of Wollongong, Wollongong, NSW, Australia

[3]   GeoQuEST Research Centre, School of Earth, Atmospheric and Life Sciences, University
     of Wollongong, Wollongong, NSW, Australia

[4]   Pusat Riset Arkeologi Prasejarah dan Sejarah, Badan Riset dan Inovasi Nasional, Jakarta,
     Indonesia

[5]   Department of Anthropology, Lakehead University, Thunder Bay, ON, Canada

[6]   Human Origins Program, National Museum of Natural History, Smithsonian Institution,
     Washington, DC, USA